Wasit Journal of Engineering Sciences

Journal homepage: https://ejuow.uowasit.edu.iq

FILM –WISE CONDENSATION OF R1234yf AND R134a REFRIGERANTS ON FINNED TUBE WITH 32 FINS PER INCH

Jasim.k Aneed[1] , Alaa R. Al-Badri[1]

Affiliations
[1]Department of Mechanical Engineering, Wasit University, Wasit, Iraq

Correspondence

Email:
jasimkhalid1989@gmail.com

Received
17-March-2022
Revised1
9- April -2022
Revised2
23-April-2022
Accepted
29-April-2022

Doi: 10.31185/ejuow.Vol10.Iss2.303

Abstract
Researchers have been motivated by the global warming challenge to develop alternatives substances to compounds that contribute to this problem. The refrigerant R134a (HFC134a) has been identified as one of the most environmentally damaging gases. As a result, the refrigerant R1234yf has been employed in air conditioning systems as a substitute to for refrigerant R134a. The condensation heat transfer coefficient (HTC) of the refrigerants R1234yf and R134a ware measured on smooth and standard finned tubes in this study. The finned tube is characterized by 32 Fins per inch (FPI) and 1 mm fin height. The condensation process was investigated at 37°C and 40°C condensing temperatures and 16°C to 28°C water inlet temperatures. The Nusselt theory accurately predicted the condensation HTCs on the smooth tube within a mean absolute percentage deviation (MAPD) of 5.3% for R134a and 4.7% for R1234yf. For the finned tube, the refrigerant R134a showed a greater HTC than R1234yf. In comparison to smooth tube, the enhancement ratio in HTC was 78% at 37 and 82% at 40°C for R134a. The enhancement ratio with R1234yf was 65% and 81% at 37 and 40 ° C, respectively. The experimental data ware compared with predictions of two previous analytical models for film condensation on finned tubes.

Keywords: Film condensation, standard finned tube, R1234yf, R134a, 32 FPI.

الخلاصة: تحدي الاحتباس الحراري حفز الباحثون لتطوير مواد بديلة للمركبات التي تساهم في هذه المشكلة. تم تحديد غاز التبريد R134a (HFC134a)) على أنه أحد أكثر الغازات إضرارًا بالبيئة. نتيجة لذلك ، تم استخدام المبرد R1234yf في أنظمة تكييف الهواء كبديل لمبرد R134a تم قياس معامل انتقال الحرارة بالتكثيف (HTC) لمواد التبريد R1234yf و R134a على أنابيب ذات زعانف ملساء وقياسية في هذه الدراسة. يتميز الأنبوب القياسي ذو الزعانف بـ ٣٢ زعنفة في البوصة (FPI) ، ويبلغ ارتفاع الزعنفة وسمكها ١ ملم و ٠.٣ ملم على التوالي. تم فحص عملية التكثيف عند ٣٧ درجة مئوية و ٤٠ درجة مئوية لدرجات حرارة تكثيف ودرجة حرارة دخول الماء من ١٦ درجة مئوية إلى ٢٨ درجة مئوية. تنبأت نظرية نسلت بدقة بتكثيف HTCs على الأنبوب الأملس بمتوسط انحراف النسبة المئوية المطلقة (MAPD) بنسبة ٥.٣٪ لـ R134a و ٤.٧٪ لـ R1234yf. مع زيادة التبريد الفرعي للجدار ، ينخفض تكثيف HTC مع انخفاض في LMTD ، يرتفع معامل انتقال الحرارة الكلي (HTC) بالنسبة للأنبوب المزعنف القياسي ، أظهر المبرد R134a قيمة HTC أكبر من R1234yf. بالمقارنة مع الأنبوب الأملس ، كانت نسبة التحسين في HTC ٧٨٪ عند ٣٧ درجة مئوية و ٨٢٪ عند ٤٠ درجة مئوية لـ R134a. كانت نسبة التحسين باستخدام R1234yf ٦٥ ٪ و ٨١٪ عند ٣٧ و ٤٠ درجة مئوية لـ ٣٢ FPI على التوالي. تمت مقارنة البيانات التجريبية مع تنبؤات نموذجين تحليليين سابقين لتكثيف الفيلم على الأنابيب ذات الزعانف القياسية.

1. INTRODUCTION

CFCs have been widely utilized in numerous refrigeration and air-conditioning applications for decades. However, they were discovered to be responsible for the depletion of the stratospheric ozone layer, and the Montreal Protocol was created in 1987 to phase out ozone - depleting compounds (UNEP, 1987). CFCs have been totally phased out in industrialized countries since 1996, and they were completely phased out by 2010 [3].To fill the void left by the phase-out of CFCs, the refrigeration and air-conditioning industries have invested much effort and resources in research and development to identify new refrigerants with a zero ozone depletion potential (ODP) [4]. HFC134a was successfully produced and utilized in vehicle air conditioners (MACs) for the past decade as a result of these efforts [5]. HFC134a has a vapor pressure and performance that is similar to CFC12 [6]. Global warming has recently become one of the most pressing concerns confronting humanity, and the Kyoto Protocol was developed in 1997 to regulate greenhouse gases including HFCs. HFC134a was discovered as one of the contaminants.

Therefore, HFC134a has been designated as one of the regulated greenhouse gases [7]. This refrigerant has a global warming potential (GWP) of 1430 [8]. So, it was planned to replace HFC134a with a more environmentally friendly refrigerant. Indeed, for environmental reasons, the EU F-Gases Regulation and MAC directive prohibit the use of HFC134a in MACs of newly manufactured automobiles beginning in 2011[9]. The use of fluorinated greenhouse gases with a GWP of more than 150 is specifically prohibited by the same MAC. R1234yf has recently been presented as a suitable replacement refrigerant for HFC134a [10]. In comparison to HFC134a, R1234yf has 0% ozone depletion potential (ODP) and outstanding Life Cycle Climate Performance (LCCP) [11]. R1234yf has a 100-year GWP of 4 [12] and so complies with EU requirements. This work aims to contribute to efforts that are oriented to provide a wide range of experimental data for film condensation of R1234yf on a standard finned tub with 32 FPI. These experimental data can be used to develop and improve the performance of the condensation process in refrigeration systems that use R1234yf. [13]. In the following, the experimental facility used for film condensation is presented.

2. EXPERIMENTAL FACILITY

An experimental system with an operating pressure of 9 bar was designed and built to measure external condensation HTCs of R1234yf and HFC134a on a smooth tube and standard finned tube (SFT). The SFT has 1260 fins per meter (32 fins per inch). The tube was made of brass and has an outside diameter of 19 mm and an effective heat transfer length of 1000 mm. The condensing temperature was set to be 37ºC and 40ºC.

The system shown in figure1 is composed of two cycles, the cold water cycle and the refrigerant cycle. The cold water cycle consists of a water cooler, water pump, flow meter, and connecting hoses between the parts. the Refrigerant cycle consists of a shell-and-tube condenser connected to an evaporator by two pipes with a diameter of 3 inches. The test section was supplied with refrigerant vapor generated by two immersed heaters of total power 4000W in the evaporator at the bottom of the apparatus. The vapor was fed into the main test section through the connecting pipe. The vapor condensed on the outside of the tested tube while cooling water flowed inside it The device is made of stainless steel to avoid corrosion as well as the system is insulated with glass wool 20 mm thick thermal insulation to avoid heat loss to the environment.

The condenser contains a charge valve to charge and refill the apertures with refrigerant, vent valve, and safety valve The inner shell diameter is (6 inches) and the length equals 1000 mm. Sight glass was installed in the middle to observe the condensation phenomenon where a light bulb is used to provide clear visualization of the condensation process on the tubes. Condenser ends were made by flanges for easy insulation of the measured tube where the condensation process takes place. During experiments, the condensate fell by gravity and was collected into the evaporator. Vapor temperature in the main test section and vapor pressure were measured by a temperature thermometer of 0.8℃ and a pressure gauge of 0.8%. error. A mass flow meter with 0.3% error and a 2 NTC10kΩ transducer with 0.2 ℃ fixed errors were used to measure the cooling water inlet and outlet temperatures.

For calculation of condensation HTC, the heat transfer rate (Q) is determined by:

$$Q = \dot{m}_{cw} C_{p,cw} \left(T_{cw,o} - T_{cw,i}\right) \tag{1}$$

The overall heat transfer coefficient is calculated by using the following equation:

$$U = \frac{Q}{A_o \; LMTD} \tag{2}$$

Where A_o the outside surface area is determined by the outside diameter of the tube, and $LMTD$ is the log-mean temperature difference, which is defined as follows:

$$LMTD = \frac{T_{cw,o} - T_{cw,i}}{ln ln \frac{T_s - T_{cw,i}}{T_s - T_{cw,o}}} \tag{3}$$

In this study, the external condensing heat transfer coefficient is separated from the overall thermal resistance as follows:

$$\frac{1}{U} = \frac{A_o}{A_i}\frac{1}{h_i} + R_w + \frac{1}{h_o} \tag{4}$$

In this equation, $R_w = \frac{D_o ln ln\left(\frac{D_r}{D_i}\right)}{2k_w}$ is the thermal resistance of tube wall.

The water side heat transfer coefficient h_i was determined using the Dittus and Boelter correlation [14] as described in Eq. 5,

$$Nu_{cw} = 0.023\, Re_{cw}^{0.8}\, Pr_{cw}^{0.4} \tag{5}$$

$$h_i = \frac{Nu_{cw} k_{cw}}{D_i} \tag{6}$$

And the condensation HTC h_o can be determined by,

$$h_o = \left(\frac{1}{U} - \frac{D_o ln ln\left(\frac{D_r}{D_i}\right)}{2K_w} - \frac{D_o}{D_i h_i}\right)^{-1} \tag{7}$$

Finally, the mean temperature of the nominal outer surface was obtained by Eq. 8,

$$T_w = T_s - \frac{Q}{A_o h_o} \tag{8}$$

and, consequently, the wall sub-cooling was determined by.

$$\Delta T = T_s - T_w \tag{9}$$

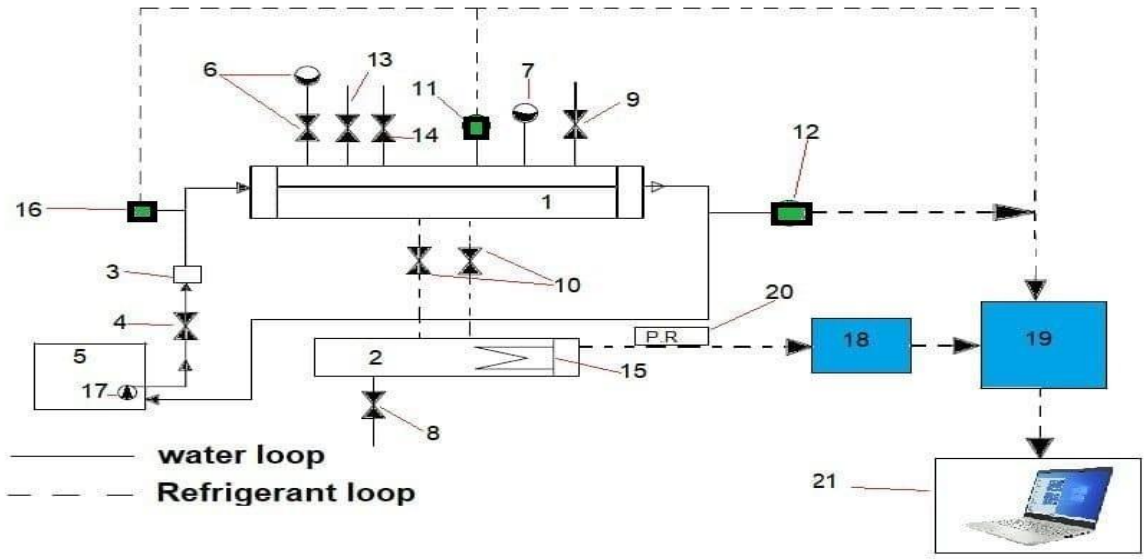

1.Condenser. 2.Evaporator 3. Flowmeter Measurement 4. Water Valve. 5. Water Cooler 6. Pr. Gauge and Manual valve. 7. Temperature Gauge. 8. Drain Valve. 9. Charge Valve. 10.Ball Valve. 11. Temperature Sensor. 12. Outlet Temperature Sensor. 13. Safety Valve. 14. Vent Valve. 15. Electrical Heater. 16. Inlet Temperature Sensor. 17. Booster Pump. 18. Power Supply. 19. Data Logger (Lab Jack). 20. Power Regulator. 21. Display Screen.

Figure1 Schematic of the Experimental setup.

Table 1 Specifications for experiment tube.

Type of Tube	Outside Diameter (mm)	Inside Diameter (mm)	Fin Height (mm)	Fin Thickness (mm)	Fin Pitch (mm)	FPI (Fins/meter)
Smooth	19	16	_	_	_	_
SFT	19	16	1	0.3	0.**8**	**32** (1**260)**

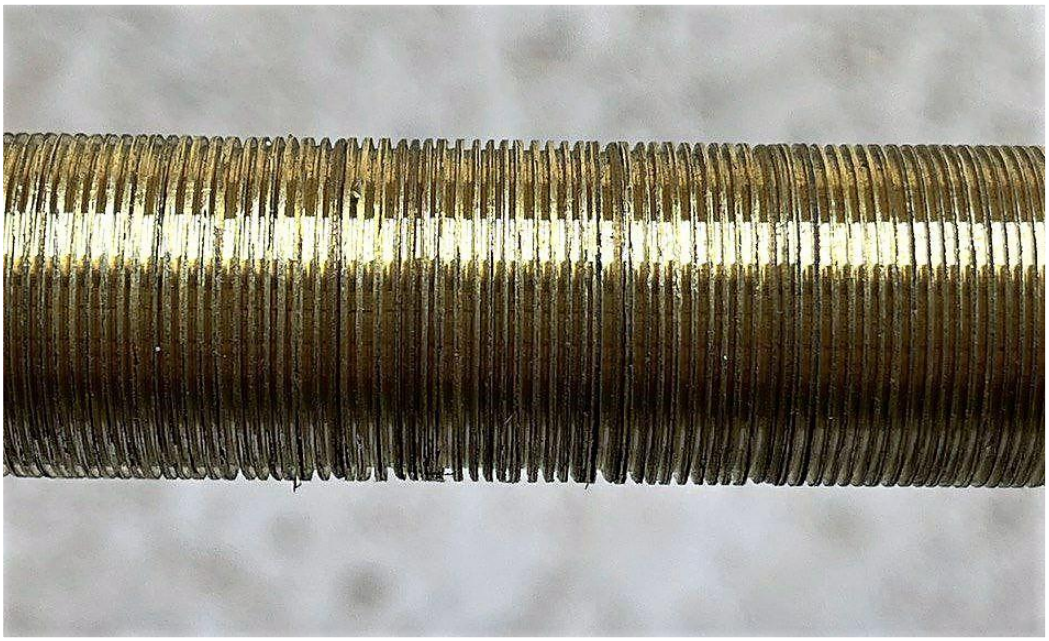

Figure 2 The SFT.

3. UNCERTAINTY ANALYSIS

The level of divergence from a true value is indicated by the amount of uncertainty in final results [23]. A fixed error, which is due to the manufacturer, and a random error, which is caused by effects during the measuring process, is both present in measurement methods. The random error was detected from the experimental results in the control and measurement laboratory at steady-state conditions, and the fixed error was minimized by a calibration process for all sensors and meters. Condensation HTC had a minimum 0.8% and maximum uncertainty of 16% as illustrate in below table 2 .

Equation (10) [24] can be used to compute the uncertainty (RE) in the result (RE) in terms of fixed and random errors.

$$\delta RE = \left[\sum_{i=1}^{n} \left(\frac{\partial RE}{\partial Xi}\partial Xi, f\right)^2 + \sum_{i=1}^{n} \left(\frac{\partial RE}{\partial Xi}\partial Xi, r\right)^2\right]^{1/2} \quad (10)$$

The two terms of the summation in equation (10) refer to the contribution

of fixed and random errors. Where $(\frac{\partial RE}{\partial Xi})$ is the partial derivative of

result (RE) to measurand (Xi), (n) is measurands number, and $(\partial Xi, f)$ and

$(\partial Xi, r)$ are the values of fixed and random errors respectively. Multi _samples uncertainty analysis is a method that used to calculate the random error ($\partial Xi, r$) from equation (11) :

$$\delta Xi, r = \frac{t\sigma_i}{\sqrt{N}} \quad (11)$$

Here, "t" can be found from "Student"s (t) distribution" depending on

The number of samples (N), which in this study was N=100 and t=2 corresponding to the confidence level 95%. (σ_i) is the stander deviation.

For the chosen samples.

Using Eqs. (1), (2) and (3), the overall HTC U can be expressed by (12)

$$U = \frac{\dot{V}_{cw}\rho_{cw}C_{P,cw}}{A_o}\, ln\, ln\left(\frac{T_{sat}-T_{cw,i}}{T_{sat}-T_{cw,out}}\right) \tag{12}$$

Where $\dot{V}_{cw}$ denoted the volumetric flow rate of cooling water which be constant value and ρ_{cw} the density. The variation in ρ_{cw} and $C_{P,cw}$ with temperature change is assumed to be insignificant for the uncertainty analysis, and therefore.

$$U = f\left(T_{sat}, T_{cw,i}, T_{cw,o}\right) \tag{13}$$

For the uncertainty of the overall HTC U, Eq. (13) should be derived with respect to $T_{sat}, T_{cw,i}\ and\ T_{cw,o}$ as follows:

$$\delta U = \left[\sum_{i=1}^{n} \left(\frac{\partial U}{\partial T_{sat}}\partial T_{sat} i,f\right)^2 + \left(\frac{\partial U}{\partial T_{cw,in}}\partial T_{cw,in} i,f\right)^2 + \left(\frac{\partial U}{\partial T_{cw,out}}\partial T_{cw,out} i,f\right)^2 + \left(\frac{\partial U}{\partial T_{sat}}\partial T_{sat} i,r\right)^2 + \left(\frac{\partial U}{\partial T_{cw,in}}\partial T_{cw,in} i,r\right)^2 + \left(\frac{\partial U}{\partial T_{cw,out}}\partial T_{cw,out} o,r\right)^2\right]^{1/2} \tag{14}$$

$$\frac{\partial U}{\partial T_{sat}} = \frac{\dot{V}_{cw}\rho_{cw}C_{P,cw}}{A_o}\frac{T_{sat}-T_{cw,out}}{(T_{sat}-T_{cw,in})\cdot(T_{sat}-T_{cw,out})} \tag{15}$$

$$\frac{\partial U}{\partial T_{cw,in}} = \frac{\dot{V}_{cw}\rho_{cw}C_{P,cw}}{A_o}\frac{1}{(T_{cw,in}-T_{sat})} \tag{16}$$

$$\frac{\partial U}{\partial T_{cw,out}} = \frac{\dot{V}_{cw}\rho_{cw}C_{P,cw}}{A_o}\frac{1}{(T_{sat}-T_{cw,out})} \tag{17}$$

Likewise, using the same variables as before, the uncertainty of the condensation HTC may be computed using the derivation of Eq. (7):

$$\delta h_o = \left[\sum_{i=1}^{n} \left(\frac{\partial h_o}{\partial T_{sat}}\partial T_{sat} i,f\right)^2 + \left(\frac{\partial h_o}{\partial T_{cw,in}}\partial T_{cw,in} i,f\right)^2 + \left(\frac{\partial h_o}{\partial T_{cw,out}}\partial T_{cw,out} i,f\right)^2 + \left(\frac{\partial h_o}{\partial T_{sat}}\partial T_{sat} i,r\right)^2 + \left(\frac{\partial h_o}{\partial T_{cw,in}}\partial T_{cw,in} i,r\right)^2 + \left(\frac{\partial h_o}{\partial T_{cw,out}}\partial T_{cw,out} o,r\right)^2\right]^{1/2} \tag{18}$$

$$\frac{\partial h_o}{\partial T_{sat}} = \frac{\partial h_o}{\partial U}\frac{\partial U}{\partial T_{sat}} \tag{19}$$

$$\frac{\partial h_o}{\partial T_{cw,in}} = \frac{\partial h_o}{\partial U}\frac{\partial U}{\partial T_{cw,in}} \tag{20}$$

$$\frac{\partial h_o}{\partial T_{cw,out}} = \frac{\partial h_o}{\partial U}\frac{\partial U}{\partial T_{cw,out}} \tag{21}$$

$$\frac{\partial h_o}{\partial U} = \left(1 - U\frac{D_o\, lnln\left(\frac{D_r}{D_i}\right)}{2K_w} - U\frac{D_o}{D_i\, h_{cw}}\right)^{-2} \tag{22}$$

$$h_{cw} = \frac{Nu\, K_w}{d_H} \tag{23}$$

$$Nu = 0.023 Re_{cw}^{0.8} pr^{0.4} \tag{24}$$

Sub, eq. (24) in eq. (23) obtain:

$$h_{cw} = \frac{0.023 Re_{cw}^{0.8} pr^{0.4} K_w}{d_H} \quad (25)$$

Table 2 Uncertainty of condensation HTC

No.	State	T_s / ℃	Range of uncertainty
1	Smooth-SFT for R134a	37℃	(0.8-11)
2	Smooth-SFT for R134a	40℃	(1-16)
3	Smooth-SFT for R1234yf	37℃	(1-11)
4	Smooth-SFT for R1234yf	40℃	(1-16)

4. RESULT AND DISCUSSION

In this work, external condensation HTCs of HFC134a and R1234yf were measured on smooth and SFT tubes at a condensing temperature of 37°C and 40°C. The flow rate of water was kept constant at 0.000187083 m^3/Sec. Inlet water temperature ranges between 16 and 28°C. In the following, experimental data of condensation heat transfer is presented, and comparisons between predictions of analytical models and our experimental data are demonstrated.

4.1 Verification of the experimental setup.

The purpose of experimental setup verification is to ensure that the experimental data obtained by the apparatus is reliable. The experimental results for the smooth tube are compared with the predicted data of Nusselt's analytical solution [3], which has been verified by several experiments in the literature.

The condensing heat transfer coefficient of pure vapor outside horizontal smooth tubes is determined by the following equation, according to the Nusselt analytical solution of vapor laminar film condensation[15].

$$h_{o,pred} = 0.728 \cdot \left(\frac{g \cdot \rho_f \cdot (\rho_f - \rho_g) h_{fg} K_f^3}{\mu_f \cdot \Delta T \cdot D_o} \right)^{1/4} \quad (26)$$

The condensing heat transfer outside the smooth tube is independent of the tube material, as shown by the above equation. It can be predicted by tube dimensions, physical properties of the condensing fluid, and the temperature difference between the wall and the vapor.

The experimental and predicted heat transfer coefficients for the smooth tube are shown in figure 3a and figure 3b. These figures. show the condensation HTC as a function of wall sub-cooling. At condensing temperatures of 37°C and 40°C, experimental and predicted values were obtained using R134a as the working fluid.

By calculating the mean absolute percentage deviation(MAPD), the predicted data is compared to experimental data. This can be determined by:

$$MAPD = \frac{100}{n} \sum_{i=1}^{n} \quad Dev_i, \quad (27)$$

$$Dev = \left| \frac{Value_{exp} - Value_{pred}}{Value_{exp}} \right| \quad (28)$$

and *n* is the number of experimental data points.

Within a mean absolute percentage deviation (MAPD) of 5.3%, the HTC predicted values are highly correlated with experimental data. As the wall sub-cooling increased, the HTC decreased. The growth in the condensate layer on the tube surface could cause this. This condensate layer adds more thermal resistance to the system, lowering the HTC. HTCs and wall sub-cooling for Nusselt and experimental data are shown in figure 3b at condensing temperatures of 37°C and 40°C, the experimental values and predicted result with R1234yf as a working fluid. The MAPD of the HTC is 4.7%, which is pretty close. This indicates that the experimental setup is suitable for achieving additional finned tube measurements.

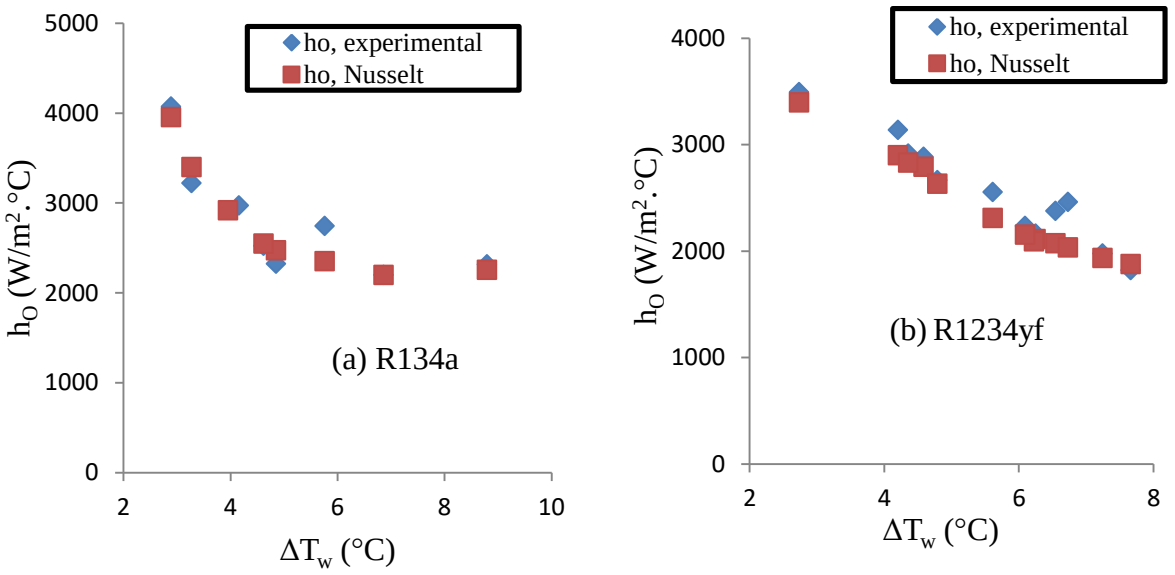

Figure 3 Comparison between predicted data and experimental data for **(a)** R134a and **(b)** R1234yf.

4.2 Experimental results for the SFT

In the following sections, experimental data of condensation heat transfer for R134a and R1234yf on the SFT are presented. Here, the corresponding condensation mode images are addressed, and the effect of condensing temperature, and the effect of the type of refrigerant on condensation performance as well as the HTC enhancement are demonstrated.

4.2.1 Condensation mode

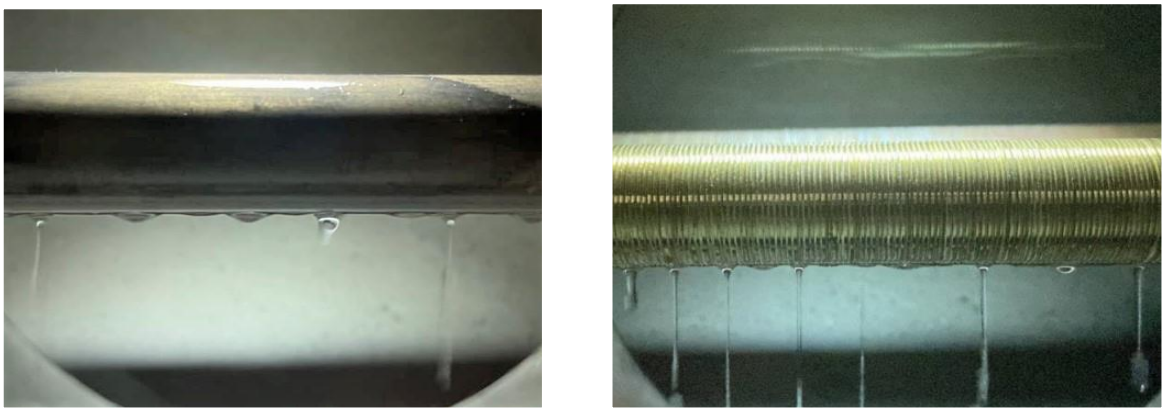

(a) Smooth,R1234yf,T_s=40°C at T_{win}=20°C **(b)** The SFT, R1234yf,T_s=40°C at T_{win}=20°C

Figure 4 Condensation Mode for R1234yf ,T_s=40°C at T_{win}=20°C **(a)** smooth and **(b)** the SFT.

Figure 4a and figure 4b display condensation process for smooth and the SFT tube respectively for working fluid R1234yf at T_{win}=20°C and condensing temperature of 40°C.

Through the figure 4 it is clear shows that the HTCs for the SFT are higher than HTCs for smooth tube, regardless the type of refrigerant and the condensing temperature.

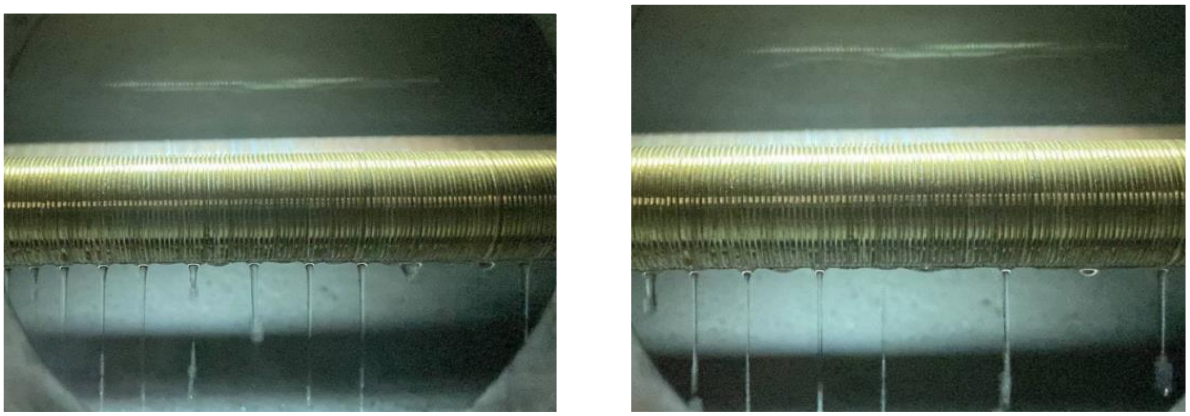

(a)SFT, R134a, T_s=37°C at T_{win}=16°C **(b)** SFT, R1234yf,T_s=37°C at T_{win}=16°C

Figure 5 Condensation Mode for the SFT ,T_s=37°C at T_{win}=16°C, **(a)** R134a and **(b)** R1234yf.

Figure 5a and figure 5b display condensation of process to working fluid R134a and R1234yf respectively for the SFT at T_{win}=16°C and condensing temperature of 37°C.

Through the figure 5 it is illustrates that the HTCs for R134a are relatively higher than HTCs for R1234yf at same condensing temperature 37 °C.

4.2.2 Effect of condensing temperature on the HTC

In the following, the relation between the HTC and the wall sub-cooling is presented with two condensing temperatures for both tested refrigerants, where figure 6 shows the comparison between condensing temperatures for R134a and R1234yf respectively. Measured data of the SFT were at a condensing temperature of 37°C and 40 °C. At each temperature, the HTC slightly decreased with the rise of the condensing temperature. a similar trend was observed for the smooth tube as well. This is because thermodynamic and transport properties affecting the condensation HTC are improved with the decrease in condensing temperature. The HTC at 37 °C showed the highest values for the tested fluids. As the condensing temperature increases, some of the properties such as liquid density and thermal conductivity affecting condensation HTC are degraded and hence HTC is decreased as well. The HTC reduces by increasing the wall sub-cooling. This is due to the augmentation in the condensate layer on the tube as mentioned earlier. This result agrees with previous studies for finned tubes[16,17,18,19,22]. However, a wide range of experimental data has to be provided to confirm the effect of condensing temperature on the condensation HTC. For both condensing temperatures, the HTC decreased with increasing the wall sub-cooling. This behavior is in line with rising condensate film thickness, which results in increased thermal resistance. The data forms an exponential relationship between wall sub-cooling and HTC despite the difference in condensing temperature among the data. This may confirm that the condensing temperature may have an insignificant effect on HTC.

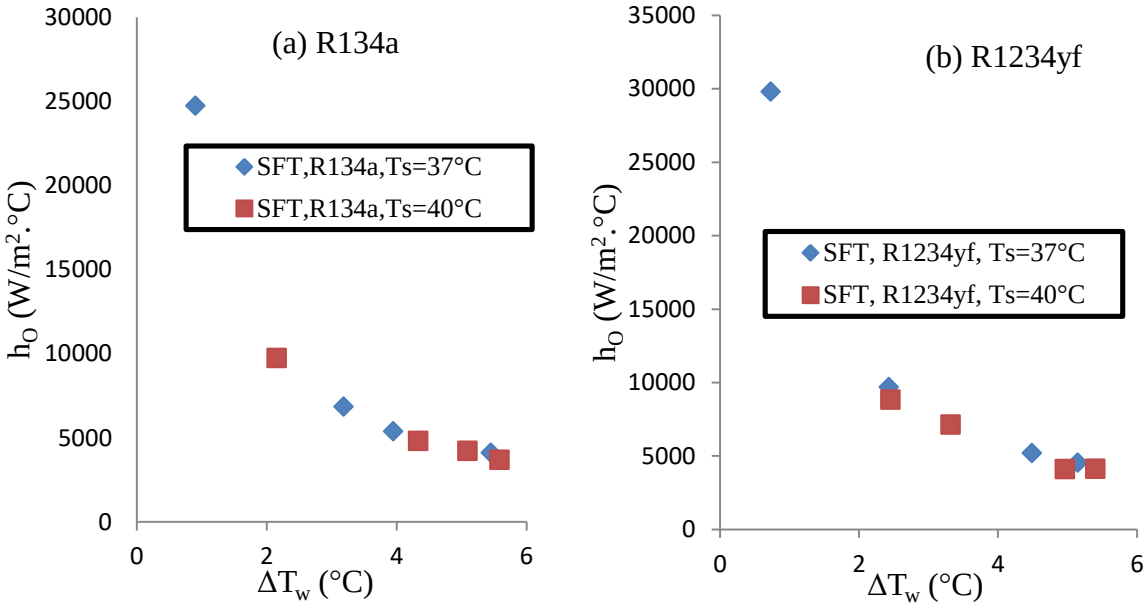

Figure 6 Comparison between condensing temperatures for **(a)** R134a and **(b)** R1234yf.

The overall HTCs U as a function of LMTD with condensing temperatures of 37°C and 40 °C are shown in figure 7 at each condensing temperature, this figure shows that U increased with the decrease in the LMTD. At each condensing temperature, the cooling water inlet temperature was set to be 16, 18, 20,22, 24,26, and 28 °C. It means that the tube side thermal resistance, in terms of varying the cooling water inlet temperature, is extremely significant in the overall heat transfer process.

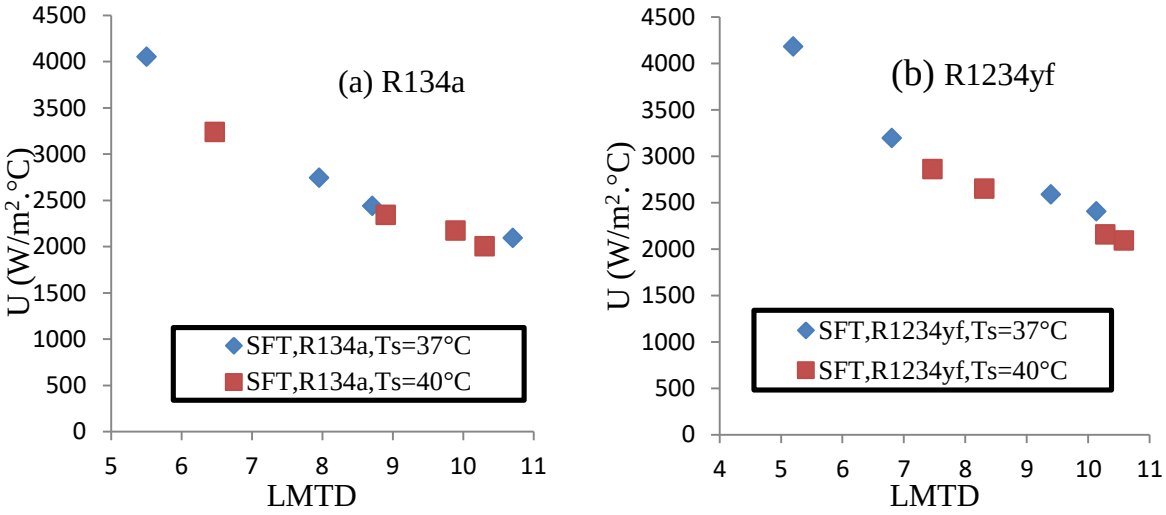

Figure 7 Comparison between condensing temperatures for **(a)** R134a and **(b)** R1234yf.

4.2.3 Effect of refrigerants

In the following, the relation between the HTC and the wall sub-cooling is presented with two types of refrigerants at condensing temperatures 37 and 40°C, for tested SFT, where figure 8a and figure 8b display a comparison between working fluid R134a and R1234yf for the SFT at condensing temperature of 37 °C. These figures show that the HTCs for R134a are relatively higher than the HTCs for R1234yf. This is in accordance with previous studies in [20] and [21], where HTCs increase with the decrease in the wall sub-cooling.

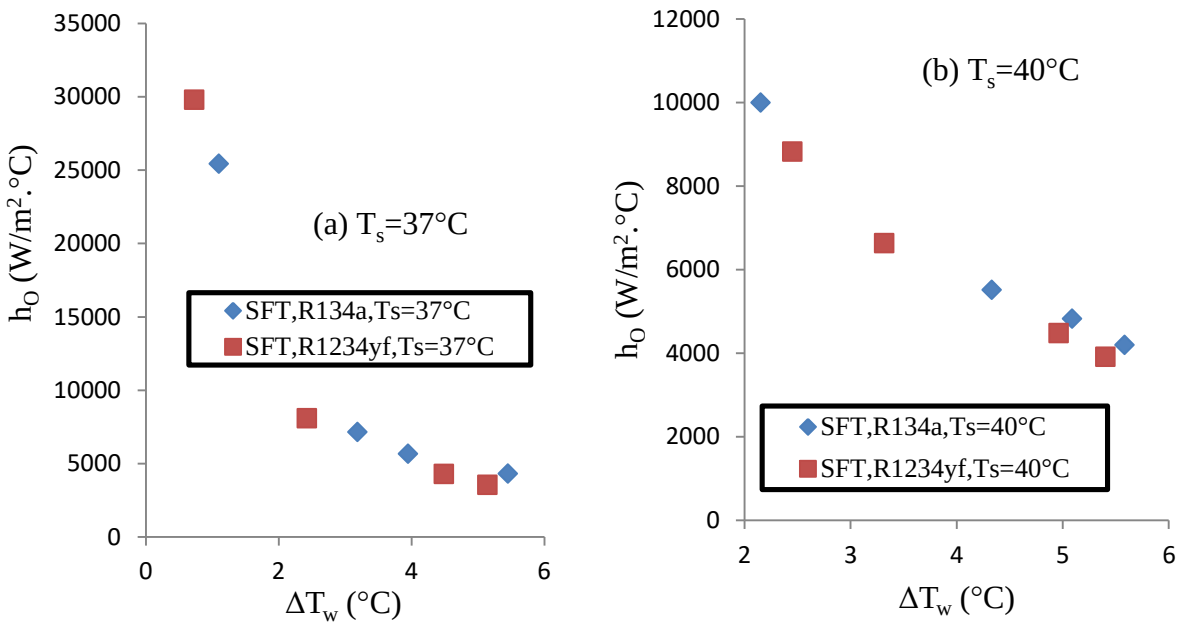

Figure 8 Comparison between working fluid R134a and R1234yf for SFT **(a)** T_s=37 °C and **(b)** T_s=40 °C.

Figure 9a and figure 9b show the change of U with LMTD for the SFT at condensing temperatures 37 and 40°C respectively. These figures show that U increases with the decrease in the LMTD. At each condensing temperature, the cooling water inlet temperature was set to be 16, 18, 20,22, 24,26, and 28 °C. It means that the tube side thermal resistance, in terms of varying the cooling water inlet temperature, is extremely significant in the overall heat transfer process.

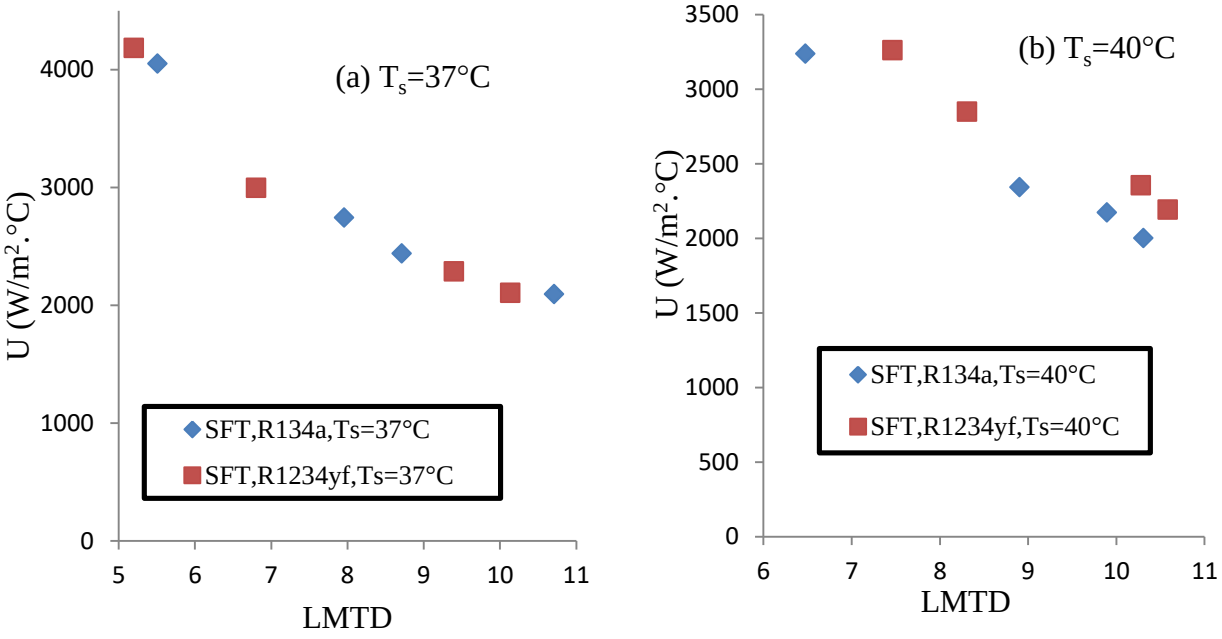

Figure 9 Comparison between working fluid R134a and R1234yf for SFT **(a)** T_s=37°C and **(b)** T_s=40 °C.

4.2.4 Comparison between smooth and finned tubes for condensation HTCs

In the following, the relation between the HTC and the wall sub-cooling is presented, where enhancement ratio is calculated between the SFT and smooth tube at condensing temperatures 37 and 40°C, for both tested refrigerants. Enhancement is obtained by dividing the difference between HTC of the finned tube and smooth tube on HTC of smooth , so that the enhancement ratio ER is equal to:

$$ER = (h_2 - h_1)/h_1 \quad (29)$$

where h_1 HTC for smooth tube and h_2 HTC for finned tube. Enhancement is the measure of the HTC improvement over the smooth tube. For calculation of enhancement factor, measured condensation HTC on a smooth tube in this study was used.

Figure 10a , figure 10b , figure 10c and figure 10d show a comparison between the SFT and smooth tube with R134a and R1234yf at constant condensing temperature 37 and 40°C respectively, after performing the calculations, the results showed the improvement percentage.

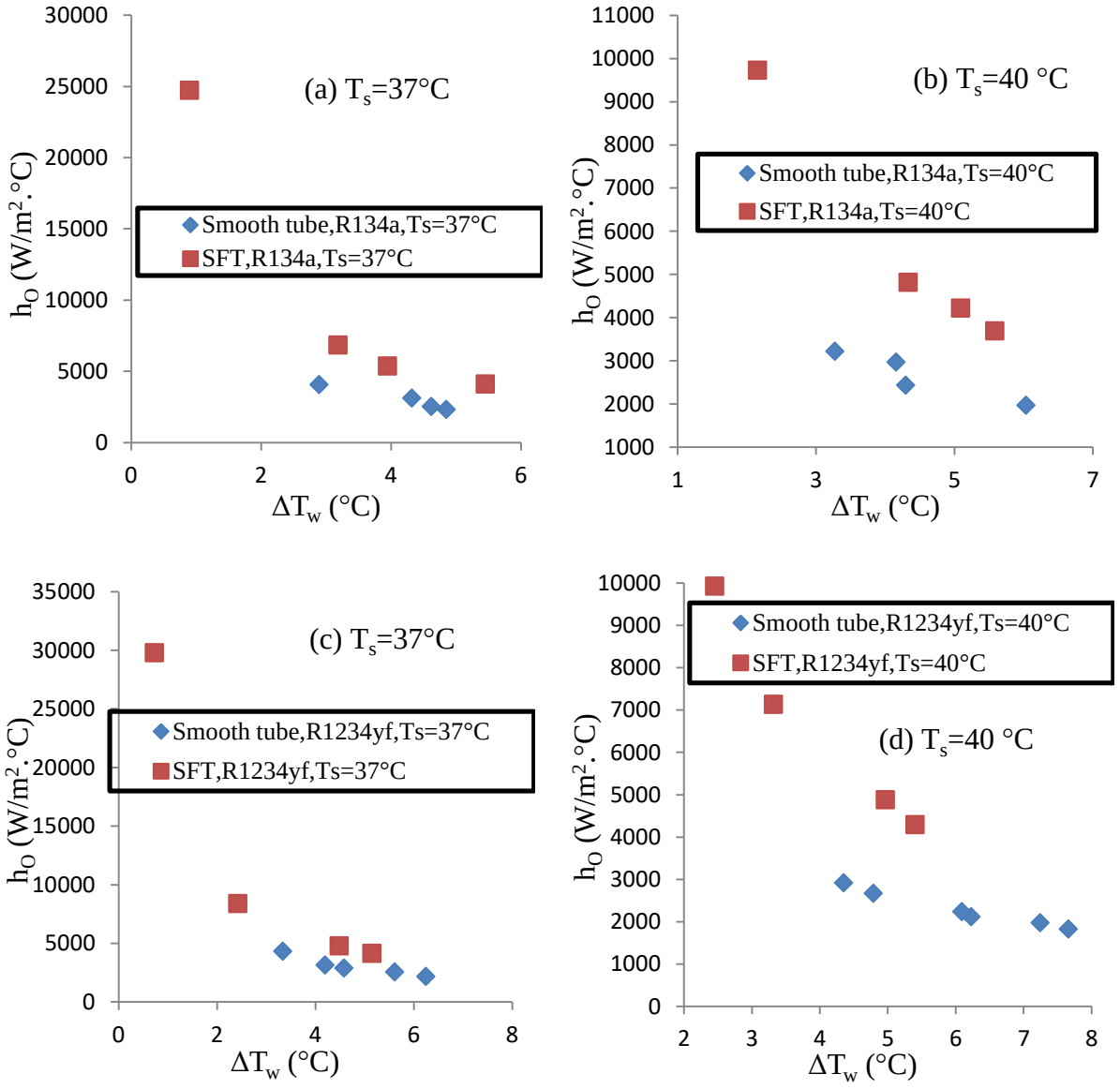

Figure 10 Comparison between smooth and SFT for R134a **(a)** T_s=37°C and **(b)** T_s=40 °C, for R1234yf **(c)** T_s=37°C and **(d)** T_s=40 °C.

that U increases with the decrease in the LMTD. At each conFigure 11a , figure 11b , figure 11c and figure 11d show a comparison between the SFT and smooth tube with R134a and R1234yf at constant condensing temperature 37 and 40°C respectively, figure 11 show the change of U with LMTD for the SFT and smooth tube at condensing temperatures 37 and 40°C respectively. These figures show densing temperature, the cooling water inlet temperature was set to be 16, 18, 20,22, 24,26, and 28 °C. It means that the tube side thermal resistance, in terms of varying the cooling water inlet temperature, is extremely significant in the overall heat transfer process.

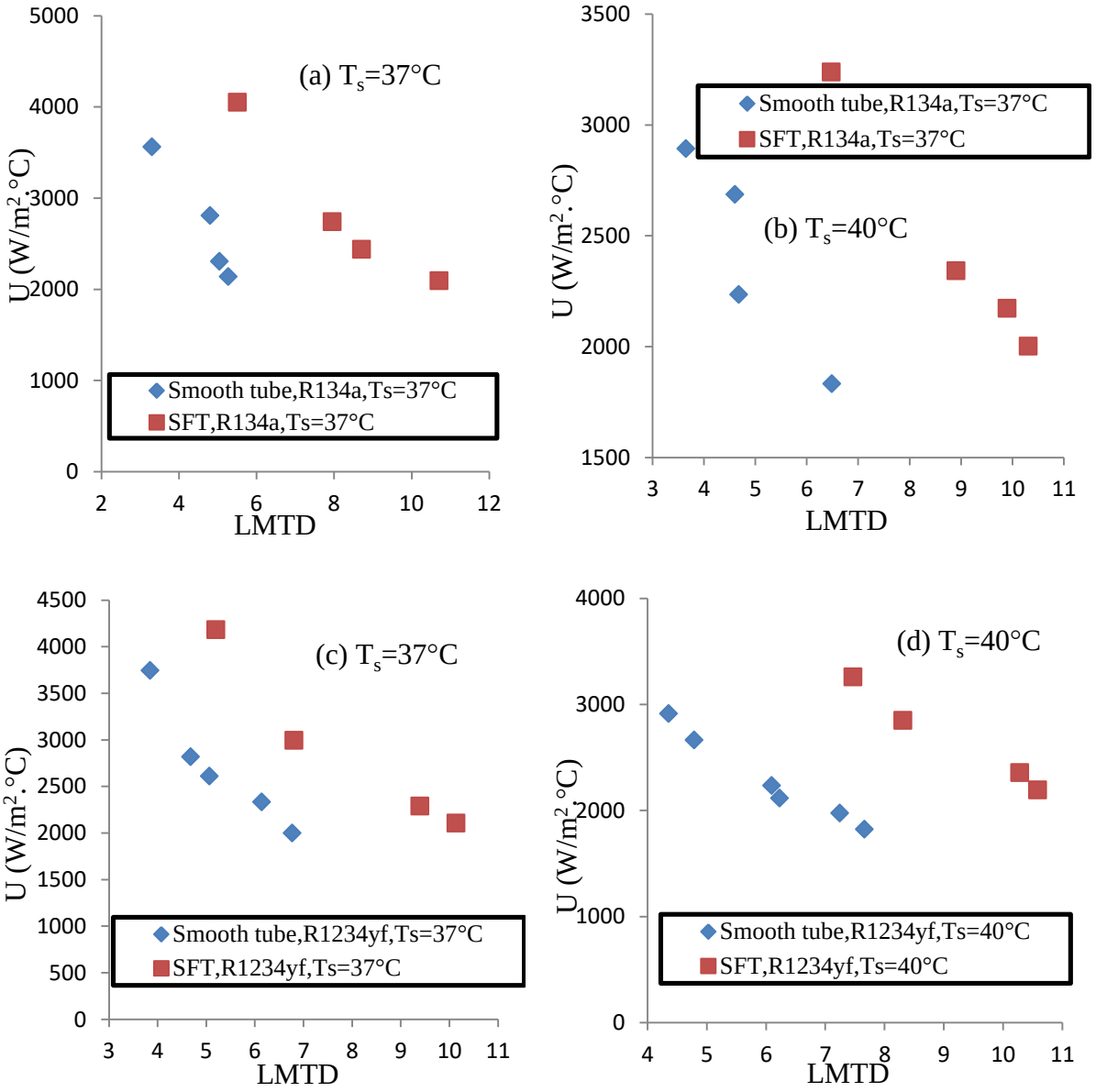

Figure 11 Comparison between smooth and SFT for R134a **(a)** T_s=37°C and **(b)** T_s=40 °C. for R1234yf **(c)** T_s=37°C and **(d)** T_s=40 °C

The below table shows the enhancement ratio for the SFT with R134a and R1234yf at 37 and 40°C.

Table3 Enhancement ratio for SFT with R134a and R1234yf at 37 and 40°C.

No.	SFT	Type of Refrigerant	T_s / °C	ER
1	32 FPI	R134a	37	78%
2			40	82%
3		R1234yf	37	65%
4			40	81%

5. COMPARISON BETWEEN PREDICTED RESULT AND EXPERIMENTAL MODEL FOR CONDENSATION HTCs

In the following, experimental data of condensation HTC is compared with predictions of previous analytical models for finned tubes. Two models are considered which are Rose model [1] and Murata and Hashizume model [2].

Figure 12a shows the prediced data of Rose model with our own experimental data. These data include measurements of refrigerants R134a and R1234yf with the SFT at 37 and 40**°C** condensing temperatures. The predicted HTC overestimates the experiments with mean absolute percentage deviation (MAPD) of 14.6%.

Figure 12b shows compassion between predations of Murata and Hashizume model with experimental data. These data at 37 and 40**°C** condensing temperatures, and R134a and R1234yf as working fluids with SFT. The expected data deviates from the experimental values with MAPD of 7.7%.

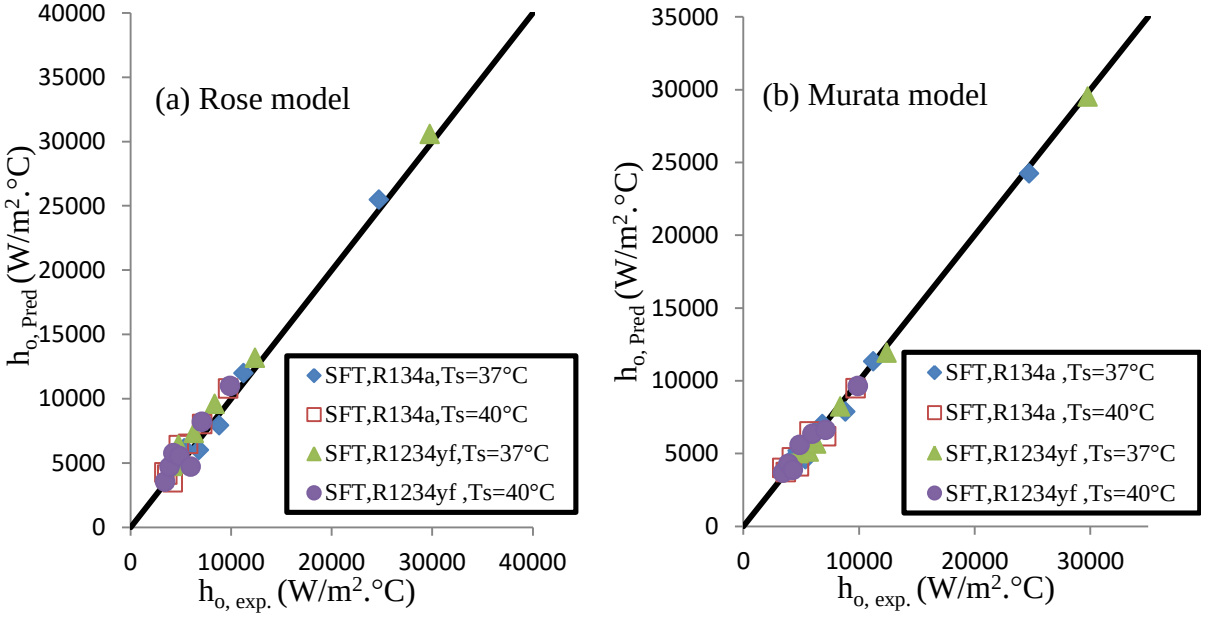

Figure 12 Comparison between experimental data and predicted data for the SFT. The predicted HTCs were determined using the model of **(a)** Rose and **(b)** Murata.

6. CONCLUSION

1. Film condensation of refrigerants R1234yf and R134a was experimentally investigated on standard finned tubes with 32 FPI. The conclusions are as follows:The Nusselt model for film condensation on horizontal tubes predicts the condensation HTCs of R134a and R1234yf on plain brass tubes with MAPD 5.3% for R134a and 4.7% for R1234yf. The experimental result shows that the Nusselt model is accurate in predicting to predict the condensation HTC of R134a and R1234yf on smooth tubes.

2. The Overall HTC U increased with the decrease in the LMTD.

3. HTCs decreased with the increase in the wall sub-cooling.

4. For the refrigerant R1234yf with the SFT, the enhancement ratio in HTC was 65% and 81% at condensing temperature of 37 and 40**°C** respectively .For the refrigerant R134a, it was 78% and 82% at condensing temperature of 37 and 40**°C** respectively.
5. The refrigerant R134a resulted in higher HTC than R1234yf for finned tube with fin height of 1mm.
6. In comparison to the experimental values for the SFT, the MAPD of predicted results for HTCs is 14.6%.for Yau et al. [1] and 7.7%. for Murata et al. [2] .
7. According to visual observations, the condensate mass flow rate of R134a is relatively higher than that of R1234yf and the condensate flow takes the form of column-droplet mode for the studied range.

REFERENCES

1. Yau, K. K., Cooper, J. R., & Rose, J. W. (1986). Horizontal plain and low-finned condenser tubes—effect of fin spacing and drainage strips on heat transfer and condensate retention.
2. Murata, K., Abe, N., & Hashizume, K. (1990). Condensation heat transfer in a bundle of horizontal integral-fin tubes. In *International Heat Transfer Conference Digital Library*. Begel House Inc..
3. Park, K. J., Kang, D. G., & Jung, D. (2010). Condensation heat transfer coefficients of HFC245fa on a horizontal plain tube. *Journal of mechanical science and technology*, ***24***(9), 1911-1917.
4. Ji, W. T., Zhao, C. Y., Lofton, J., Li, Z. Y., Zhang, D. C., He, Y. L., & Tao, W. Q. (2018). Condensation of r134a and r22 in shell and tube condensers mounted with high-density low-fin tubes. *Journal of Heat Transfer*, ***140***(9).
5. Ji, W. T., Zhao, C. Y., Zhang, D. C., Li, Z. Y., He, Y. L., & Tao, W. Q. (2014). Condensation of R134a outside single horizontal titanium, cupronickel (B10 and B30), stainless steel and copper tubes. *International Journal of Heat and Mass Transfer*, ***77***, 194-201.
6. Jung, D., Kim, C. B., Cho, S., & Song, K. (1999). Condensation heat transfer coefficients of enhanced tubes with alternative refrigerants for CFC11 and CFC12. *International Journal of Refrigeration*, ***22***(7), 548-557.
7. Al-Badri, A. R., Gebauer, T., Leipertz, A., & Fröba, A. P. (2013). Element by element prediction model of condensation heat transfer on a horizontal integral finned tube. *International Journal of Heat and Mass Transfer*, ***62***, 463-472.
8. Gebauer, T., Al-Badri, A. R., Gotterbarm, A., El Hajal, J., Leipertz, A., & Fröba, A. P. (2013). Condensation heat transfer on single horizontal smooth and finned tubes and tube bundles for R134a and propane. *International Journal of Heat and Mass Transfer*, ***56***(1-2), 516-524.
9. Ji, W. T., Zhao, C. Y., Lofton, J., Li, Z. Y., Zhang, D. C., He, Y. L., & Tao, W. Q. (2018). Condensation of r134a and r22 in shell and tube condensers mounted with high-density low-fin tubes. *Journal of Heat Transfer*, ***140***(9).
10. Longo, G. A., & Zilio, C. (2012). HFO1234yf condensation inside a brazed plate heat exchanger.
11. Ji, W. T., Lu, X. D., Yu, Q. N., Zhao, C. Y., Zhang, H., & Tao, W. Q. (2020). Film-wise condensation of R-134a, R-1234ze (E) and R-1233zd (E) outside the finned tubes with different fin thickness. *International Journal of Heat and Mass Transfer*, ***146***, 118829.
12. Al-Badri, A. R., Bär, A., Gotterbarm, A., Rausch, M. H., & Fröba, A. P. (2016). The influence of fin structure and fin density on the condensation heat transfer of R134a on single finned tubes and in tube bundles. *International Journal of Heat and Mass Transfer*, ***100***, 582-589.
13. Park, K. J., Kang, D. G., & Jung, D. (2011). Condensation heat transfer coefficients of R1234yf on plain, low fin, and Turbo-C tubes. *International journal of refrigeration*, *34*(1), 317-321.
14. Dirker, J., & Meyer, J. P. (2002). Heat transfer coefficients in concentric annuli. *J. Heat Transfer*, ***124***(6), 1200-1203.
15. Nusselt, W. (1916) De oberflachenkondensation des waserdampfes. *Z. VDI*, Frankfurt, **60**, 541-546, 569-575.
16. Fernández-Seara, J., Uhía, F. J., Diz, R., & Dopazo, A. (2010). Condensation of R-134a on horizontal integral-fin titanium tubes. *Applied Thermal Engineering*, ***30***(4), 295-301.
17. Ji, W. T., Mao, S. F., Chong, G. H., Zhao, C. Y., Zhang, H., & Tao, W. Q. (2019). Numerical and experimental investigation on the condensing heat transfer of R134a outside plain and integral-fin tubes. *Applied Thermal Engineering*, ***159***, 113878.
18. Christians, M., Habert, M., & Thome, J. R. (2010). Film condensation of R-134a and R-236fa,

part 1: experimental results and predictive correlation for single-row condensation on enhanced tubes. *Heat transfer engineering*, ***31***(10), 799-808.

19. Christians, M., Habert, M., & Thome, J. R. (2010). Film condensation of R-134a and R-236fa, part 1: experimental results and predictive correlation for single-row condensation on enhanced tubes. *Heat transfer engineering*, ***31***(10), 799-808.
20. Al-Badri, A. R., Rausch, M. H., Leipertz, A., & Fröba, A. P. (2014). Effect of fin pitch, fin height, and bundle depth on condensation of R134a, R1234yf, and R1234ze in bundles of integral finned tubes. In *Proceedings of the DKV-Conference, Duesseldorf, Germany*.
21. Rand A. AL-Taee, Alaa R. Al-Badri, (2021). Experimental Study on Film Condensation of R1234 outside Finned Tubes. Journal of Mechanical Engineering Research and Development, ***44***(9), 319-327.
22. Ji, W. T., Mao, S. F., Chong, G. H., Zhao, C. Y., Zhang, H., & Tao, W. Q. (2019). Numerical and experimental investigation on the condensing heat transfer of R134a outside plain and integral-fin tubes. *Applied Thermal Engineering*, ***159***, 113878.
23. Moffat, R. J. (1988). Describing the uncertainties in experimental results. *Experimental thermal and fluid science*, ***1***(1), 3-17.
24. K. H. K Murata, K., Abe, N., & Hashizume, K. (1990). Condensation heat transfer in a bundle of horizontal integral-fin tubes. In *International Heat Transfer Conference Digital Library*. Begel House Inc.

Nomenclature

Symbol	Definition	Units SI
A	Area	m^2
$\mathbf{C_P}$	Specific heat	$KJ.\mathrm{kg}^{-1}.\ K^{-1}$
D	Diameter	m
g	Gravitational acceleration	$m.s^{-2}$
h	Heat transfer coefficient	$W.m^{-1}.k^{-1}$
$\mathbf{h_{fg}}$	Latent heat	$kJ.\mathrm{kg}^{-1}$
K	thermal conductivity	$W.m^{-1}.k^{-1}$
$\dot{\boldsymbol{m}}$	Mass flow rate	kg. s^{-1}
Nu	Nusselt number	-
Pr	Prandtl number	-
Q	Heat transfer rate	W
q	Heat flux	W.m^{-2}
R	Thermal resistance	kW^{-1}
Re	Reynolds number	-
S	Fin spacing	m
U	Overall heat transfer coefficient	$W.m^{-1}.k^{-1}$
ΔT	Wall sub-cooling	$K\ or$°C
T	temperature	$K\ or$°C

Greek Symbol

Symbol	Definition	Units SI
ρ	Density	kg. m^{-3}
μ	Viscosity	pa s

Subscripts

Symbol	Definition
cw	Cooling water
cw, i	Cooling water inlet
cw, o	Cooling water outlet
f	Liquid
g	vapor
I	Inner
O	Outer
pred	Predicted
r	Fin root
s	Saturation of vapor
w	Water

Abbreviations

Symbol	Definition
FPI	Fins per inch
GWP	Global warming potential
HTC	Heat transfer coefficient
LCCP	Life cycle climate performance
MAC	Automobile air conditioner
MAPD	Mean absolute percentage deviation
ODP	Ozone depletion potential
SFT	Standard finned tube